Fast neutrino flavor conversion modes in multidimensional core-collapse supernova models: The role of the asymmetric neutrino distributions

Sajad Abbar,[1,2] Huaiyu Duan,[2] Kohsuke Sumiyoshi,[3] Tomoya Takiwaki,[4] and Maria Cristina Volpe[1]

[1]*Astro-Particule et Cosmologie (APC), CNRS UMR 7164, Université Denis Diderot, 75205 Paris Cedex 13, France*

[2]*Department of Physics & Astronomy, University of New Mexico, Albuquerque, New Mexico 87131, USA*

[3]*National Institute of Technology, Numazu College, Ooka 3600, Numazu, Shizuoka 410-8501, Japan*

[4]*National Astronomical Observatory of Japan, Osawa, Mitaka, Tokyo 181-8588, Japan*

(Received 7 November 2019; accepted 5 February 2020; published 20 February 2020)

A dense neutrino gas, such as the one anticipated in the supernova environment, can experience fast neutrino flavor conversions on scales much shorter than those expected in vacuum probably provided that the angular distributions of ν_e and $\bar{\nu}_e$ cross each other. We perform a detailed investigation of the neutrino angular distributions obtained by solving the Boltzmann equations for fixed matter profiles of some representative snapshots during the postbounce phase of core-collapse supernovae in multidimensional calculations of a 11.2 $M_\odot$ and a 27 $M_\odot$ progenitor model. Although the 11.2 $M_\odot$ model features $\nu_e - \bar{\nu}_e$ angular crossings and the associated fast modes at different time snapshots, the 27 $M_\odot$ model does not show any crossings within the decoupling region. We show that this can be understood by studying the multipole components of the neutrino distributions. In fact, there is a higher chance for the occurrence of $\nu_e - \bar{\nu}_e$ angular crossings for the zones where the multipole components of the neutrino distributions are strong enough. We also show that there can exist more than one crossing between the angular distributions of ν_e and $\bar{\nu}_e$. In addition, apart from the crossings within the neutrino decoupling region, there is a class of $\nu_e - \bar{\nu}_e$ angular crossings that appears very deep inside the protoneutron star.

DOI: 10.1103/PhysRevD.101.043016

I. INTRODUCTION

A massive star with a mass larger than 8–10 $M_\odot$ can end its life in a core-collapse supernova (CCSN) explosion [1]. During this process, a huge amount of energy is released of which almost 99% is in the form of neutrinos of all flavors. Although an infinitesimal fraction of the released energy is in the form of electromagnetic radiation, only ∼0.01%, it is already enough to allow a CCSN to outshine its host galaxy.

Neutrinos can experience flavor oscillations as they propagate. Neutrino oscillations can, at least in principle, notably impact the physics of CCSNe. First, it can affect the heavy elements nucleosynthesis occurring in the SN environment by modifying the n/p ratio through the weak reactions $\bar{\nu}_e + p \rightleftharpoons n + e^+$ and $\nu_e + n \rightleftharpoons p + e^-$ [2]. Neutrino oscillations can modify the ν_e and $\bar{\nu}_e$ spectra which in turn modifies the rate of these reactions.

Moreover, the SN dynamics can also be affected by neutrino oscillations. Although the mechanism of the explosion is not well understood yet, a popular mechanism proposed in the late 1980s is the so-called *delayed explosion mechanism* in which the explosion is aided by absorbing a fraction of the energy of neutrinos emitted from the SN core [3–5]. Likewise, neutrino oscillations can modify the neutrino energy deposition by changing ν_e and $\bar{\nu}_e$ spectra.

Finally, to confront theory with observations, predictions of the neutrino fluxes and spectra are crucial for future observations of CCSNe neutrino signals and the measurement of the neutrino diffuse background [6–11].

The phenomenon of neutrino oscillations in dense neutrino media, such as the one expected in the SN environment, is remarkably different from the one in vacuum and matter. Neutrinos can experience collective flavor evolution in a dense neutrino gas owing to the fact that the coherent forward scattering by the background neutrino gas can now play a role in neutrino evolution because of the large neutrino number densities [12–16].

Most of the initial understanding of neutrino flavor evolution in the SN environment was based on the stationary spherically symmetric neutrino bulb model [13] in which neutrinos are emitted isotropically from the surface of the neutrinosphere. The salient feature of the results obtained in this model is the existence of the flavor swapping phenomenon in which ν_e ($\bar{\nu}_e$) exchanges its spectra with ν_x ($\bar{\nu}_x$) for a range of neutrino energies [14,15,17–20]. This is indeed a consequence of collective neutrino oscillations in the SN environment.

However, neutrinos could also undergo the so-called *fast* flavor conversions on scales as short as a few cm in the densest regions of the SN core [21–36]. Unlike the

 © 2020 American Physical Society

traditional collective modes that occur on scales determined by the neutrino vacuum frequency $\omega = \Delta m^2/2E$ [$\sim\mathcal{O}(1)$ km for a 10 MeV neutrino and atmospheric mass splitting], fast modes occur on scales $\sim G_{\rm F}^{-1} n_\nu^{-1}$ with n_ν and $G_{\rm F}$ being the neutrino number density and the Fermi coupling constant, respectively. It is believed that a necessary condition for the occurrence of fast modes is the presence of crossing(s) in the angular distribution of electron lepton number carried by neutrinos (ELN) [24,26,28,29]. It has been shown that in the presence of ELN crossings, fast modes can arise due to the merging of two noncollective modes [33] and $G_{\rm F} n_\nu$ can play the role of ω, which in turn allows for the existence of flavor conversion modes on relatively short scales [29].

Fast modes, if they exist, can remarkably influence the physics of CCSNe. On the one hand, they can lead to neutrino flavor conversions within the SN zones that have long been thought to be the realm of scattering processes (occurring on scales $\sim G_{\rm F}^{-2} E^{-2} n_{\rm B}^{-1}$ with $n_{\rm B}$ being the baryon number density) [31,37]. On the other hand, they can result in flavor conversions close to the surface of the protoneutron star (PNS) where it can be more influential. This is important since (if fast modes are absent) calculations have shown so far that significant neutrino flavor conversions are not likely to occur close to the surface of the PNS, in spite of the existence of flavor instabilities therein [38–42]. In fact, the unstable modes can turn stable before growing significantly due to the rapid variations of the physical conditions during the neutrino propagation [39,43]. However, fast modes can change this picture by occurring on short enough scales and therefore not being bothered by the rapid variations of the physical conditions.

Although such ELN crossings were not considered in the bulb model calculations (neutrinos were assumed to be emitted isotropically from the surface of a single sharp neutrinosphere), they are speculated to exist in realistic SN models. This simply arises from the fact that ν_e and $\bar{\nu}_e$ decouple at different radii. Thus, one might simply expect that ELN crossings should be unavoidable in the SN environment [22,23].

Nevertheless, one-dimensional SN simulations have not shown such ELN crossings during the early stages of CCSNe within the shock region [44,45] (note, however, that they might still exist in the preshock SN region [46]). Although the angular distributions of $\bar{\nu}_e$'s are normally more peaked than that of ν_e's in the forward direction, the large difference between the number densities of ν_e and $\bar{\nu}_e$ hinders the occurrence of ELN crossings. However, this story can be changed in multidimensional (multi-D) SN models. Indeed, recent multi-D SN simulations have shown that the neutrino distributions can be highly asymmetric in the presence of lepton-emission self-sustained asymmetry (LESA) [47–55]. Such asymmetric neutrino distributions can significantly help increasing the chance of the occurrence of ELN crossings by providing SN zones with smaller difference between $n_{\bar{\nu}_e}$ and n_{ν_e} [56].

However, most of the state-of-the-art multi-D SN simulations do not provide such detailed angular information of neutrinos due to the simplifications made in the neutrino transport. SN simulations in which full neutrino angular distributions are available have become accessible just recently [57–59]. The first investigation of the occurrence of ELN crossings in multi-D SN models was reported in Ref. [56] in which the Boltzmann equations were solved for a number of fixed SN matter profiles and a number of ELN crossings and the associated fast modes were found in both two-dimensional (2D) and three-dimensional (3D) calculations of an 11.2 $M_\odot$ progenitor model. Subsequently, the results of a self-consistent 2D SN simulation (solving the Boltzmann equations and hydrodynamics simultaneously) were reported in which ELN crossings were not observed for the selected few spatial points [60]. Although both of the computations were performed for an 11.2 $M_\odot$ progenitor model, the employed equations of state (EOS) were different. This can have profound consequences for the occurrence of ELN crossings, as is discussed in this paper.

In this study, we explore the neutrino angular distributions obtained by solving the Boltzmann equations for several fixed SN matter profiles that are representative snapshots taken from multi-D SN simulations. Following our previous study [56], we present a more detailed investigation of the ELN crossings in an 11.2 $M_\odot$ progenitor model. Furthermore, we present and analyze our results of the calculations of a 27 $M_\odot$ progenitor models in which no ELN crossings within/above the neutrino decoupling region were observed (Sec. III). We also discuss the possibility of the existence of a class of ELN crossings in very deep regions well inside the PNS (Sec. IV).[1] By performing linear stability analysis (Sec. II), we show that fast modes associated with the ELN crossings can lead to flavor conversion rates as large as several e-folds per nanosecond (Sec. III).

II. LINEAR STABILITY ANALYSIS

The state of a neutrino traveling with momentum $\mathbf{p}$ can be specified by its flavor density matrix $\varrho_{\mathbf{p}}(t, \mathbf{x})$ [63] at each time t and point $\mathbf{x}$, and its flavor evolution in the absence of the collision term is governed by the Liouville-Von Neumann mean-field equation of motion [63–67]

$$i(\partial_t + \mathbf{v}\cdot\nabla)\varrho_{\mathbf{p}} = [\mathrm{H}_{\mathbf{p}}, \varrho_{\mathbf{p}}], \tag{1}$$

with $\mathbf{v}$ being the neutrino velocity that in the spherical coordinate can be defined as $\mathbf{v} = (\sin\theta_\nu\cos\phi_\nu, \sin\theta_\nu\sin\phi_\nu, \cos\theta_\nu)$ for a neutrino with emission angles $(\theta_\nu,\ \phi_\nu)$.

[1] Refs. [61,62] appeared while this manuscript was in the last stages of its preparation. In Ref. [62], the authors report similar occurrence of deep ELN crossings inside the PNS.

Also, $\mathrm{H}_{\mathbf{p}} = \mathrm{H}_{\mathrm{vac}} + \mathrm{H}_{\mathrm{mat}} + \mathrm{H}_{\nu\nu,\mathbf{p}}$ is the total Hamiltonian where, in the two-flavor scenario,

$$\mathrm{H}_{\mathrm{vac}} \approx \frac{\eta\omega}{2}\begin{bmatrix} 1 & 0 \\ 0 & -1 \end{bmatrix} \tag{2}$$

$$\mathrm{H}_{\mathrm{mat}} = \frac{\lambda}{2}\begin{bmatrix} 1 & 0 \\ 0 & -1 \end{bmatrix}, \tag{3}$$

with $\eta = +1(-1)$ for the inverted (normal) mass ordering and $\lambda = \sqrt{2}G_{\mathrm{F}}n_e$ with n_e being the electron number density [68,69], where it is assumed that $\theta_{\mathrm{v}} \ll 1$ and strong matter currents are absent. Finally,

$$\mathrm{H}_{\nu\nu,\mathbf{p}} = \sqrt{2}G_{\mathrm{F}}\int \frac{\mathrm{d}^3\mathbf{p}'}{(2\pi)^3}(1 - \mathbf{v}\cdot\mathbf{v}')(\varrho_{\mathbf{p}'} - \bar{\varrho}_{\mathbf{p}'}) \tag{4}$$

is the contribution from neutrino-neutrino refraction [70–72]. Here, the flavor density matrices can be written as [73]

$$\varrho = \frac{f_{\nu_e} + f_{\nu_x}}{2}\mathbb{1} + \frac{f_{\nu_e} - f_{\nu_x}}{2}\begin{bmatrix} s & S \\ S^* & -s \end{bmatrix}, \tag{5}$$

where S and s are some complex and real quantities, respectively, and f_ν is the (prior to oscillation) neutrino occupation number, so that the neutrino number and flux densities are

$$n_\nu = \int \frac{\mathrm{d}^3p}{(2\pi)^3} f_\nu(\mathbf{p}),$$
$$\mathbf{j}_\nu = \int \frac{\mathrm{d}^3p}{(2\pi)^3} f_\nu(\mathbf{p})\mathbf{v}, \tag{6}$$

respectively. Likewise, $\bar{\nu}$ quantities can be defined with respect to $f_{\bar{\nu}_e}$ and $f_{\bar{\nu}_x}$.

In the presence of fast modes, Eq. (1) turns out to be approximately blind to the neutrino energy (at least in the linear regime). Thus, one can set $\omega = 0$ and drop the energy dependency of ϱ and integrate over the neutrino energy. It then proves to be useful to define the neutrino electron lepton number (ELN) as [24]

$$G_{\mathbf{v}} = \sqrt{2}G_{\mathrm{F}}\int_0^\infty \frac{E_\nu^2\mathrm{d}E_\nu}{(2\pi)^3}[f_{\nu_e}(\mathbf{p}) - f_{\bar{\nu}_e}(\mathbf{p})], \tag{7}$$

assuming $f_{\nu_x}(\mathbf{p}) = f_{\bar{\nu}_x}(\mathbf{p})$.

One can then linearize Eq. (1) by keeping the terms of order $\mathcal{O}(|S_{\mathbf{v}}|)$ or larger [24,73,74],

$$i(\partial_t + \mathbf{v}\cdot\nabla)S_{\mathbf{v}} = (\epsilon_0 + \mathbf{v}\cdot\boldsymbol{\epsilon})S_{\mathbf{v}} - \int \mathrm{d}\Gamma_{\mathbf{v}'}(1 - \mathbf{v}\cdot\mathbf{v}')G_{\mathbf{v}'}S_{\mathbf{v}'}, \tag{8}$$

where $\mathrm{d}\Gamma_{\mathbf{v}'}$ is the differential solid angle in the direction of $\mathbf{v}'$, $\epsilon_0 = \lambda + \int \mathrm{d}\Gamma_{\mathbf{v}'}G_{\mathbf{v}'}$, and $\boldsymbol{\epsilon} = \int \mathrm{d}\Gamma_{\mathbf{v}'}G_{\mathbf{v}'}\mathbf{v}'$.

Because Eq. (8) is linear in $S_{\mathbf{v}}$, it has the normal solutions of the form

$$S_{\mathbf{v}} = Q_{\mathbf{v}}e^{-i\Omega t + i\mathbf{K}\cdot\mathbf{x}}. \tag{9}$$

Collective neutrino oscillations can then lead to significant flavor conversions if there exist solutions with complex Ω and/or $\mathbf{K}$.

Furthermore, if the neutrino and antineutrino distributions possess axial symmetry, it is convenient to integrate neutrino quantities over ϕ_ν and work with ϕ_ν-integrated quantities,

$$f_\nu(\theta_\nu) = \int \frac{E_\nu^2\mathrm{d}E_\nu\mathrm{d}\phi_\nu}{(2\pi)^3} f_\nu(\mathbf{p}) \tag{10}$$

and

$$G(\theta_\nu) = \int_0^{2\pi} \mathrm{d}\phi_\nu G_{\mathbf{v}}. \tag{11}$$

To study fast modes in the SN environment, we then assumed a homogenous neutrino gas at each SN zone for which we adopted the local angular distributions from the SN model. This could be justified by the fact that fast modes are expected to occur on scales much smaller than that of the SN core. Thus, one can safely ignore the global geometry of the core and focus on the local physics of the problem. However, this approximation is valid as long as the neutrino instabilities occur on scales well inside the considered SN zone.

It should be noted that a significant amount of backward traveling neutrinos within the neutrino decoupling region leads to the existence of spatial fast instabilities even without ELN crossings [24,26,29]. However, to have growing instabilities, the existence of temporal instability with complex Ω is necessary [26,75]. Therefore, one can focus on the temporal modes having in mind that the spatial instabilities are only important to determine the absolute or convective nature of the growing instabilities [76].

III. OCCURENCE OF ELN CROSSINGS IN MULTI-D SN MODELS

The neutrino distributions in this study were obtained by the calculations of neutrino transport for the fixed backgrounds (density, temperature and electron fraction) of 2D/3D matter profiles in the supernova core. The time evolution of the neutrino distributions was followed until a stationary state for the neutrino quantities was reached.

The Boltzmann equation was solved directly in the full phase space to obtain the neutrino energy and angle distributions. The multiangle multienergy neutrino transport in 2D/3D space was carried out by using the S_n method

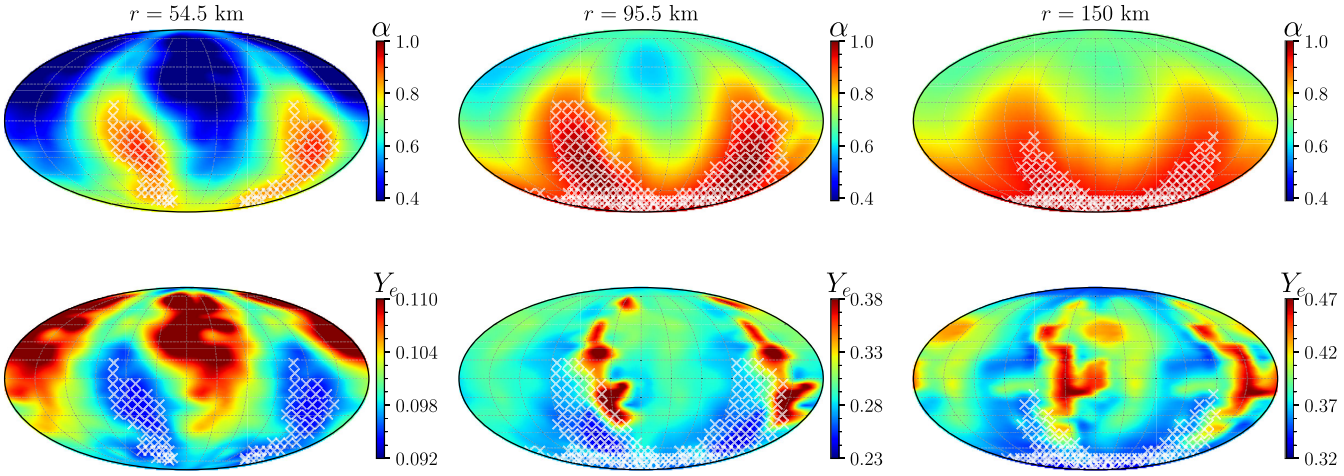

FIG. 1. The Mollweide projection of α (upper panels) and the electron fraction Y_e (lower panels) of the 3D 11.2 $M_\odot$ progenitor model calculations in the $t = 200$ ms snapshot at $r = 54.5$, 95.5 and 150 km, respectively. Crosses indicate the ELN crossings. Note that the color scales may not be the same for different panels. At this time, neutrinos decouple from matter at radii $\gtrsim$50 km, highly depending on their flavors and energies.

and the time evolution was handled by the time implicit method. Further details of our numerical method can be found in Refs. [57,58].

In the neutrino transport, three neutrino species, namely, ν_e, $\bar{\nu}_e$ and ν_x, were handled where ν_x represents ν_μ and ν_τ and their antiparticles. The microphysics used in the evaluation of the neutrino transport is the same as the one in Refs. [56,58] where the neutrino reaction rates for emission, absorption, scattering and pair processes were taken mostly from Ref. [77] and its extensions. In addition, the Lattimer and Swesty EOS [78] was used to be consistent with the original supernova simulations.

We adopted multi-D supernova profiles of the two progenitor models of an 11.2 $M_\odot$ (both 2D and 3D) and a 27 $M_\odot$ (only 3D) [58,79,80]. The spatial resolutions of the Boltzmann calculations were set to be (256, 64, 1) and (256, 64, 32) for the numbers of spatial zones (N_r, N_Θ, N_Φ) in spherical coordinates for the 2D and 3D models, respectively, where a maximum radius of 2613 km from the original simulations was reached. For the neutrino momentum space, a resolution of (14, 6, 12) was employed for $(N_{E_\nu}, N_{\theta_\nu}, N_{\phi_\nu})$ in both 2D and 3D calculations. In addition, to examine the angular convergence of the calculations, we performed similar neutrino transport calculations with a higher resolution of $N_{\theta_\nu} = 36$ for the snapshots of the 2D 11.2 $M_\odot$ progenitor model at $t = 150$ and 200 ms.

For the 11.2 $M_\odot$ progenitor model, three representative snapshots at $t = 100$, 150 and 200 ms from the original 2D and 3D simulations were selected for which the Boltzmann equations were solved. As mentioned in Ref. [56], ELN crossings within/above the decoupling region were only observed in the snapshot at $t = 200$ ms in the 2D calculations, whereas they were found in all of the time snapshots in the 3D calculations. For instance, in the snapshot at $t = 200$ ms, the ELN crossings above the neutrinosphere appear first at $r \simeq 46$ km within a relatively narrow region in the southern hemisphere (Fig. 1). As the radius increases, the crossings zone expands initially because the neutrino distributions get more peaked in the forward direction. However, it gets narrower again at larger radii and disappears at $r \sim 200$ km. As is discussed later, this disappearance of the ELN crossings could be an artificial result of the limited angular resolution of the neutrino transport calculations.

As pointed out in Ref. [56], the ELN crossings zones appear to be correlated with the zones where the $\nu_e - \bar{\nu}_e$ asymmetry parameter,

$$\alpha = \frac{n_{\bar{\nu}_e}}{n_{\nu_e}},$$

is close to 1. This, indeed, is not coincidental and can be understood as follows. In the SN environment, the angular distribution of $\bar{\nu}_e$ is normally more peaked in the forward direction than that of ν_e because they decouple at smaller radii. One then might be tempted to assume that the occurrence of ELN crossings in CCSNe is inevitable. However, if the $\nu_e - \bar{\nu}_e$ asymmetry is large, the occurrence of ELN crossings could be remarkably suppressed. In fact, a larger $\nu_e - \bar{\nu}_e$ asymmetry means a more separated ν_e and $\bar{\nu}_e$ angular distributions and therefore less chance for the occurrence of ELN crossings. Thus, ELN crossings are more likely to occur within the zones with small $\nu_e - \bar{\nu}_e$ asymmetries (α close to 1).

The pattern in α (and the neutrino distributions) is obviously (anti-) correlated with a similar pattern in the electron fraction Y_e (Fig. 1). Figure 2 shows that it first

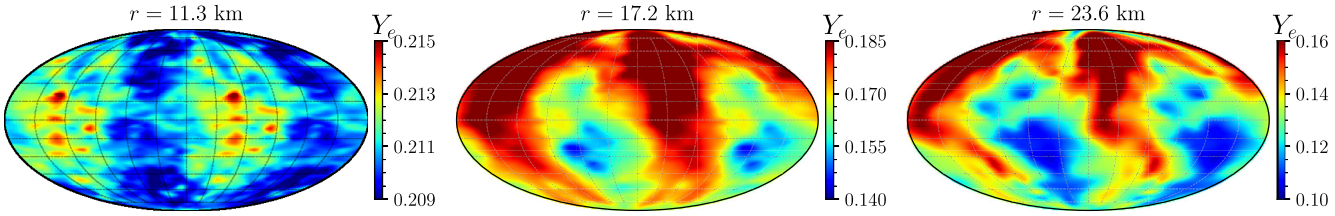

FIG. 2. The Mollweide projection of the electron fraction Y_e of the 3D 11.2 $M_\odot$ progenitor model calculations in the $t = 200$ ms snapshot at $r = 11.3$, 17.2 and 23.6 km, respectively. The pattern observed in Fig. 1 first appears very deep inside the PNS. Note that the color scales may not be the same for different panels.

appears very deep inside the PNS. As pointed out in Ref. [47], in the case of LESA convectional flows in the PNS could generate asymmetries in the neutrino fluxes. In our 3D models, the pattern in Y_e shows up first at $r \sim 11$ km and becomes more distinct at larger radii. The pattern in Y_e can then be associated with a similar pattern in α because more (less) ν_e's ($\bar{\nu}_e$'s) are emitted where Y_e is larger.

For the 27 $M_\odot$ progenitor model, three representative snapshots at $t = 150$, 200 and 250 ms from the original 3D simulations were selected. In contrast to the case of the 11.2 $M_\odot$ progenitor model, no ELN crossings above the neutrinosphere were found in this case. A few representative Mollweide projections of α at different radii (corresponding to the ones in Fig. 1 for the 11.2 $M_\odot$ progenitor model) are plotted in Fig. 3. Although it shows some slight spatial variations, the value of α within/above the neutrino decoupling region is always much smaller than one in this model which in turn provides a little chance for the occurrence of ELN crossings.

During the early stages of a CCSN, (the average of) α tends to be relatively small. This can seriously hinder the occurrence of ELN crossings in the SN environment. In particular, no ELN crossings within the shock region have been found in 1D SN models so far [44,45] except in the preshock SN region [46]. However, the situation can be different in multi-D SN models where the neutrino distributions can be spatially asymmetric due to multi-D hydrodynamics. In fact, although the average value of α is thought to be similar in 1D and multi-D SN models, the existence of multipole structures in α in the latter can allow for regions with large α's which increases the chance for the occurrence of ELN crossings. Figure 4 presents the $l = 0$, 1, 2 multipole components of the spherical harmonics decomposition of α, defined as

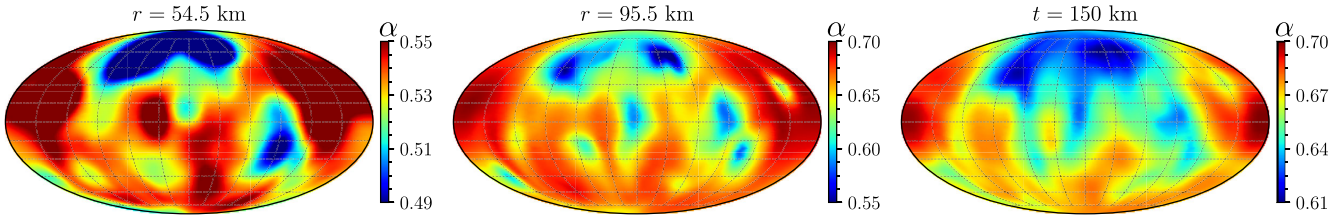

FIG. 3. The Mollweide projection of α of the 3D 27 $M_\odot$ progenitor model calculations in the $t = 200$ ms snapshot at $r = 54.5$, 95.5 and 150 km, respectively. Note that the color scales are not the same for different panels.

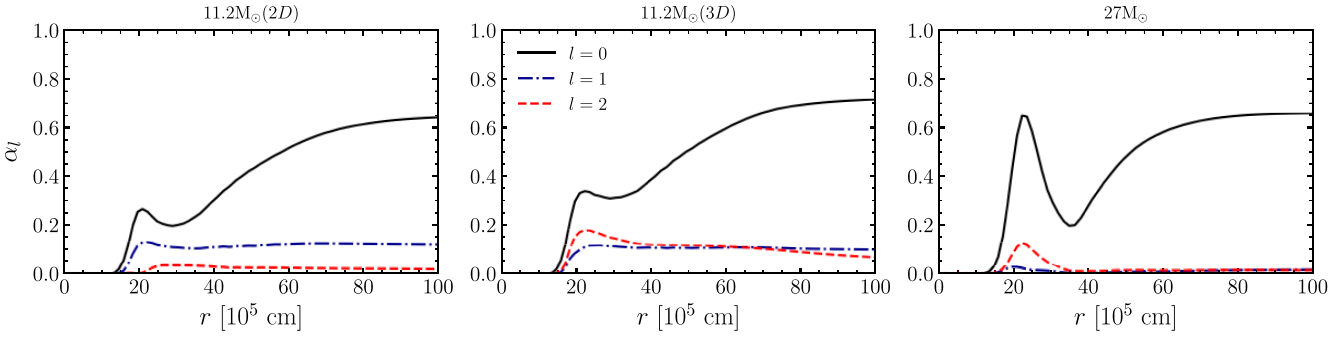

FIG. 4. Radial evolution of the multipole components of α Eq. (12) for the $t = 200$ ms snapshots. In 2D and 3D 11.2 $M_\odot$ progenitor models, strong dipole and quadrupole components in α exist; while in the 27 $M_\odot$ one, these are only found inside the PNS.

$$\alpha_l = \left(\sum_{m=-l}^{l} \left| \int \frac{d\Omega}{\sqrt{4\pi}} Y^*_{lm}(\Theta,\Phi)\alpha(\Theta,\Phi) \right|^2 \right)^{1/2}. \quad (12)$$

As one can see, both the 2D and the 3D 11.2 $M_\odot$ progenitor models show strong dipole and quadrupole components in α. On the other hand these are weak in the 27 $M_\odot$ progenitor model, except for a small region inside the PNS where ELN crossings exist (see Sec. IV). This provides an explanation on why there is no ELN crossings within/above the neutrino decoupling region for this model. Furthermore, while in the 2D calculations the dipole component is dominant in all of the snapshots, it is the quadrupole term that is stronger, at least at smaller radii, in all of the 3D snapshots.

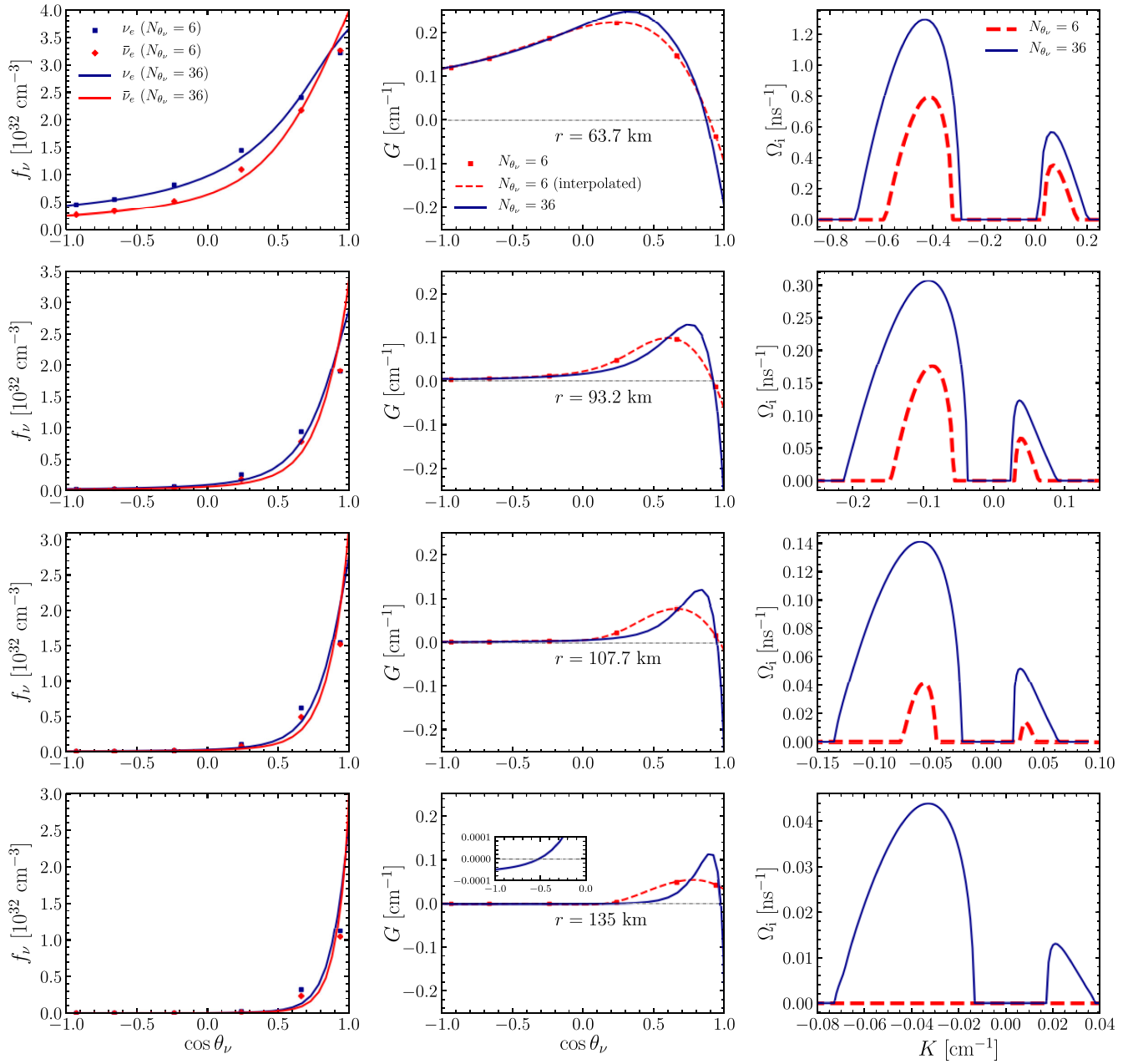

FIG. 5. Angular distributions of neutrinos f_ν (left), ELN (middle), as functions of the angular variable θ_ν, and the corresponding eigenvalues Ω_i (right panels), Eqs. (8) and (9), as functions of the real wave number K. The results correspond to fast neutrino oscillation modes propagating in the radial direction, at the four different radii $r = 63.7$, 93.2, 107.7 and 135 km. The angular distributions are extracted from the spatial point with $\cos\Theta = 0.99$ in the 2D model in the $t = 200$ ms snapshot. The zoomed-up subplot indicates the shallow crossing at $\cos\theta_\nu \simeq -0.56$ in the calculation with $N_{\theta_\nu} = 36$. A similar shallow crossing exists in the calculations with $N_{\theta_\nu} = 6$ but the low angular resolution does not allow for a definite recognition of it. At this time, the neutrinospheres of different flavors are located at radius ~50–70 km (see Fig. 4 of Ref. [56]).

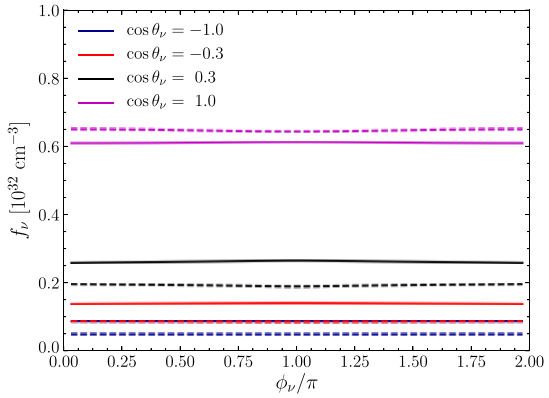

FIG. 6. Neutrino angular distributions as functions of ϕ_ν for ν_e (solid) and $\bar{\nu}_e$ (dashed) and at different $\cos\theta_\nu$ values [Eq. (13)]. The results are obtained from the 2D calculations of the $t = 200$ ms 11.2 $M_\odot$ progenitor model, for the spatial zone at $r = 61.8$ km and $\cos\Theta = 0.98$. The asymmetry in ϕ_ν turns out to be small for the spatial zones with ELN crossings.

A few representative ϕ_ν-integrated angular distributions of ν_e, $\bar{\nu}_e$ and the corresponding ELN [Eqs. (10) and (11)] are presented in Fig. 5 for the $t = 200$ ms 2D 11.2 $M_\odot$ progenitor model. The angular distributions with $N_{\theta_\nu} = 6$ and $N_{\theta_\nu} = 36$ are in a relatively good agreement. The only exception is at larger radii, where the calculations with smaller number of angle bins fail (expectedly) to capture the angular structures at small emission angles. In fact, as the radius gets larger, the ELN crossings get narrower because the neutrino angular distributions become more forward peaked. Therefore, higher angular resolution is needed to capture them. This implies that the disappearance of the ELN crossings at larger radii could be an artefact of the low angular resolution of the neutrino transport calculations. The average neutrino quantities are in much better agreement between the two calculations with different resolutions, the values of n_ν and α differing at most by 2%–3%.

Moreover, we noticed that there are cases where the ELN distributions exhibit two crossings. This phenomenon seemingly occurs at larger radii where the neutrino angular distributions are highly peaked in the forward direction. As shown in Fig. 5, at r = 135 km there is a first shallow crossing at negative values of $\cos\theta_\nu$ and a second one at $\cos\theta_\nu \simeq 1$.

Besides the analysis of the neutrino angular distributions, we performed a linear stability analysis and solved Eq. (8) to find the growth rates of the unstable modes [Eq. (9)] at each spatial zone. The calculations assume axial symmetry for the neutrino gas. In fact, the neutrino angular distributions

$$f_\nu(\theta_\nu, \phi_\nu) = \int \frac{E_\nu^2 \mathrm{d}E_\nu}{(2\pi)^3} f_\nu(\mathbf{p}) \tag{13}$$

are highly symmetric in ϕ_ν at all of the spatial zones for which ELN crossings were observed, as illustrated by Fig. 6. Overall, the deviation from axial symmetry in the zones with ELN crossings turns out to be smaller than a few percent in both 2D and 3D models. However, one should keep in mind that this can be changed for rotating models where the angular distributions can be quite asymmetric in ϕ_ν [81]. As mentioned earlier, the temporal instability is necessary to have growing perturbations. The complex eigenvalues associated with the temporal fast modes are plotted in Fig. 5. The corresponding exponential growth rates can be as large as several e-folds per nanoseconds and tend to be larger for the wider ELN crossings.

Our results suggest that even the more accessible calculations with low angular resolution might provide a quite reliable estimate of the presence of ELN crossings and correspondingly fast modes. This is corroborated by the fact that we did not find false ELN crossings in the calculations with lower angular resolution and the associated instability growth rates provided a reasonable estimate of the results based on higher angular resolution. Obviously, one cannot exclude that in a dynamic self-consistent CCSN simulation, the prompt convection might be more suppressed if the angular resolution is too low [59].

IV. ELN CROSSINGS INSIDE THE PNS

Apart from the ELN crossings occurring within/above the decoupling region of neutrinos, there is another class of ELN crossings that can appear in deep regions inside the PNS. In our calculations, such ELN crossings exist at radii in the range 20–28 km.

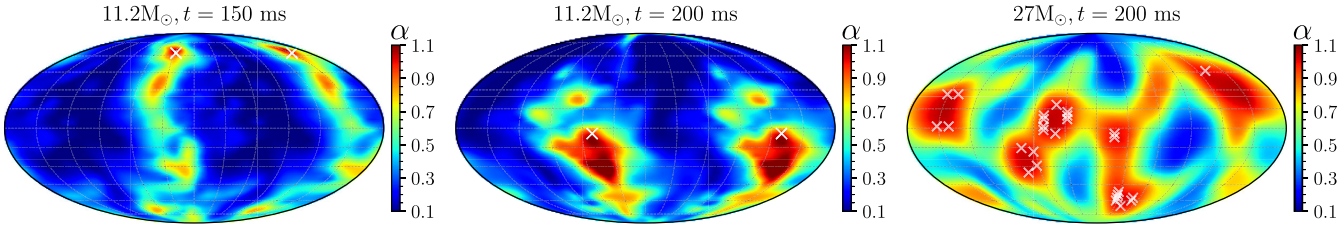

FIG. 7. The Mollweide projection of α of the 3D calculations at $r = 23.6$ km in different time snapshots. The few crosses indicate ELN crossings inside the PNS. Note that the crossings inside the PNS are not as abundant as the ones within the decoupling region and they only exist within the zones where α is extremely close to 1.

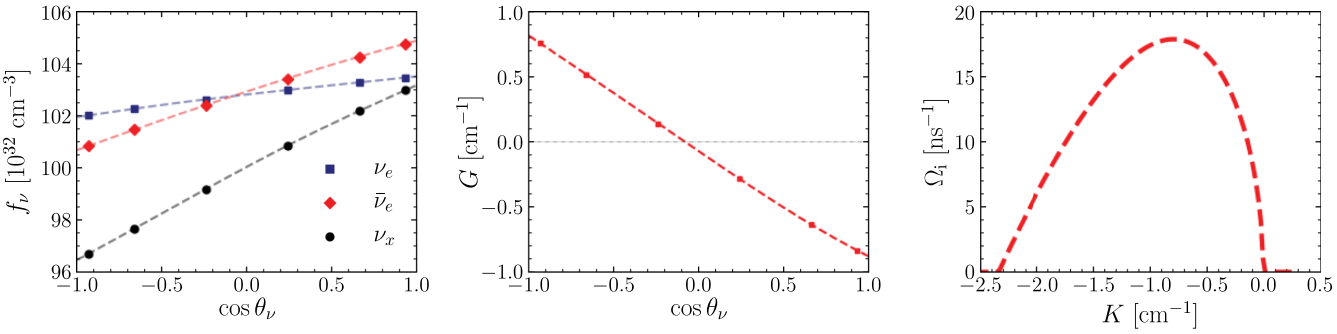

FIG. 8. Angular distributions, as functions of θ_ν, for ν_e, $\bar{\nu}_e$ and ν_x (left), ELN (middle) and the corresponding eigenvalues Ω_i (right panel), as a function of the real wave number K. Interpolated values are also shown (dashed lines). The results are for the fast modes propagating in the radial direction, at the spatial zone with $r = 26.4$, $\cos\Theta = 0.40$ and $\Phi = 0.72\pi$ deep inside the PNS, for which an ELN crossing exists. The calculations are for 3D 11.2 $M_\odot$ progenitor model and the $t = 200$ ms snapshot. Note that the neutrino angular distributions are very close to each other and highly nondegenerate, with $n_{\bar{\nu}_e}/n_{\nu_e} = 1.001$ and $n_{\nu_x}/n_{\nu_e} = 0.972$.

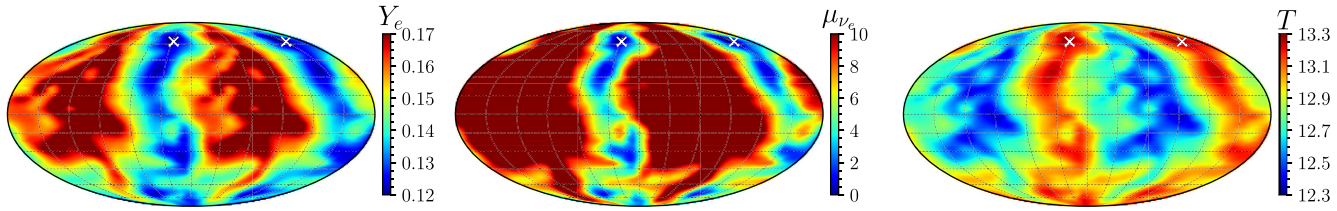

FIG. 9. The Mollweide projection of the electron fraction Y_e, the electron neutrino chemical potential μ_{ν_e} and the temperature T of the 3D 11.2 $M_\odot$ progenitor model calculations at $r = 23.6$ km in the $t = 150$ ms snapshot corresponding to the very left panel in Fig. 7. μ_{ν_e} and T are both in MeV.

For the 2D 11.2 $M_\odot$ progenitor model, only two ELN crossings at ~25 km exist in the snapshot at $t = 100$ ms, while they appear in all 3D snapshots. As for the 27 $M_\odot$ progenitor model, the ELN deep crossings are present in the $t = 150$ and 200 ms snapshots (Fig. 7). Note that there exist no ELN crossings within the decoupling region for this progenitor model.

Since the neutrino angular distributions are significantly isotropic inside the PNS, the deep crossings can only exist if α is extremely close to 1, i.e., the ν_e and $\bar{\nu}_e$ angular distributions are very close to each other (Fig. 8). Note that if α has values both below and above 1, it is very likely to have this sort of ELN crossing provided that the spatial resolution is high enough. With this in mind, it is safe to say that the key question here is whether such hot spots (as in Fig. 7) do actually show up in more realistic SN simulations. It should also be noted that such ELN crossings do not necessarily occur at $\cos\theta_\nu \simeq 1$.

The reason for having SN zones for which $\alpha \simeq 1$ can be understood as follows. As shown in Fig. 9, the neutrino gas is very nondegenerate ($\mu_\nu/T \simeq 0$) at the ELN crossing points inside the PNS. In fact, the chemical potentials of ν_e and $\bar{\nu}_e$ become similar at these points, i.e., $\mu_{\nu_e} \simeq \mu_{\bar{\nu}_e} \simeq 0$ ($\mu_{\nu_e} = \mu_p - \mu_n + \mu_e$). This happens because $\mu_p - \mu_n$ can almost cancel μ_e at these SN zones where Y_e is minimum.[2] Thus, a correlation exists between Y_e and μ_{ν_e}. In addition, the temperature has its maximum value at these points. As mentioned in Ref. [53], this (anti-) correlation between Y_e and T can be explained by noting that in spite of the asymmetric neutrino distributions, the density and pressure tend to maintain their spherical symmetry. This simply arises from the sphericality of the gravitational potential, which mainly governs the variations of these quantities. Therefore, one should expect higher temperatures within the zones where Y_e is lower to keep the combination of thermal and electron degeneracy pressures constant ($p = p(\rho, T, Y_e)$).

Although the existence of the deep ELN crossings surprisingly allows for the occurrence of fast modes inside the PNS, there are two essential points that should be kept in mind. First, one can indeed observe large flavor conversion rates for all the SN zones where α is extremely close to 1, even for those for which the ELN crossings are absent. For example, in an isotropic homogeneous monoenergetic neutrino gas initially consisting of ν_e and $\bar{\nu}_e$ (bipolar model), for $|\alpha - 1| \ll 1$, the exponential growth rate governing flavor evolution is [82,83]

$$\Omega_i \approx \sqrt{2\mu\omega}, \tag{14}$$

for

[2]We thank Shoichi Yamada for valuable conversation about this possibility.

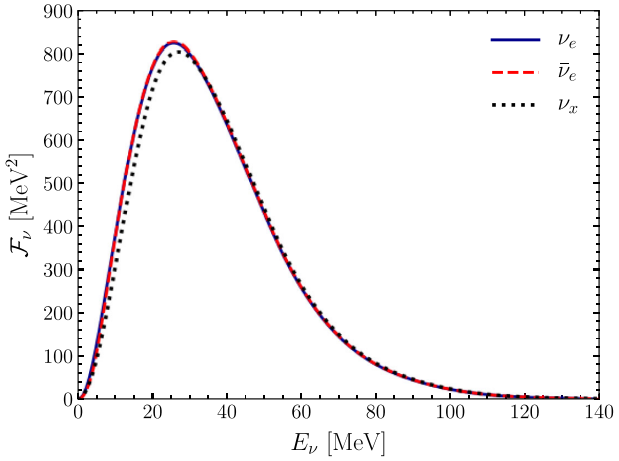

FIG. 10. The neutrino energy distributions at the spatial point corresponding to the one in Fig. 8.

$$\frac{2}{(1+\sqrt{\alpha})^2} < \mu/\omega < \frac{2}{(1-\sqrt{\alpha})^2}, \tag{15}$$

for $\eta = 1$.[3] This implies that even in the bipolar model (in the absence of ELN crossings), there can exist unstable slow modes on scales $\propto G_{\rm F}^{-1/2} n_\nu^{-1/2}$ at spatial zones where $\alpha \simeq 1$. Such scales can be $\lesssim 1$ m (compare with fast modes occuring on scales $\sim G_{\rm F}^{-1} n_\nu^{-1} \lesssim 10$ cm) for these SN zones inside the PNS. This is much shorter than the collisional scales ($\lesssim \mathcal{O}(10^2)$ m) therein. Therefore, having large neutrino flavor conversion rates for nondegenerate SN zones is not unique to fast modes.

Secondly, the neutrino distributions are significantly similar for all neutrino species within these zones meaning that not only $n_{\nu_e} \simeq n_{\bar{\nu}_e} \simeq n_{\nu_x}$ (Fig. 8), but also the energy distributions

$$\mathcal{F}_\nu(E_\nu) = \int {\rm d}\Gamma_{\mathbf{v}} E_\nu^2 f_\nu(\mathbf{p}), \tag{16}$$

are very similar for different neutrino species (Fig. 10). Consequently, neutrino oscillations should not have significant impact on the flavor content of the neutrino gas.

V. DISCUSSION AND CONCLUSION

To assess the possibility of the occurrence of ELN crossings and the associated fast neutrino flavor conversion modes in the SN environment, we have studied neutrino angular distributions obtained by solving the Boltzmann equations for fixed matter profiles of some representative snapshots during the postbounce phase of CCSNe in 2D and 3D for an 11.2 $M_\odot$ and a 27 $M_\odot$ (only 3D) progenitor models.

[3]In the case of slow modes, the exponential growth rate is $\sim\sqrt{\omega\mu}$. However, unless α is extremely close to 1, $\mu \sim \omega$ which means $\Omega_{\rm i} \sim \omega$. One can observe a similar instability for $\eta = -1$ by breaking the axial/spatial symmetry.

For the 11.2 $M_\odot$ progenitor model, ELN crossings were observed in both 2D and 3D models. It turns out that they tend to occur within the SN zones where the $\nu_e - \bar{\nu}_e$ asymmetry parameter, α, is very close to 1, as in Ref. [56]. Unlike the 1D SN modes in which α is thought to be globally small during the early stages of a CCSN, zones with large α's could exist in multi-D SN models in the presence of a spatially asymmetric neutrino distributions due to multi-D hydrodynamics. The reason is that in spite of having similar average values of α to 1D models, multi-D SN models can feature larger α's in zones where α is significantly larger than its averaged value.

The pattern in α is (anti-) correlated with a similar pattern in Y_e (and T) that appears very deep inside the PNS and is thought to be caused by the convectional flows therein. This is closely related to LESA [47–55] in which strong dipole structure exists in the neutrino distributions, which can be preceded by strong higher multipole structures at earlier times. Our study suggests that if the multipole structures (either dipole at later times or higher multipoles at earlier times) are strong enough, they can lead to the existence of zones with significantly large α's and a good chance for the occurrence of ELN crossings. However, at this point in time it is not very clear how the fast modes propagate from these zones to other regions. Note also that such asymmetric structures in α do not necessarily need to come from LESA. In general any significant asymmetry in the neutrino distributions, self-sustained with relatively constant direction (as in LESA) or not, can increase the chance for the occurrence of ELN crossings in the SN environment.

To see how increasing the neutrino angular resolution can affect the occurrence of ELN crossings, we performed calculations with higher angular resolution with $N_{\theta_\nu} = 36$ in 2D for our 11.2 $M_\odot$ progenitor model. It turns out that not only do the calculations with lower resolution not produce any false ELN crossings, but they also can provide a relatively good estimate of the flavor conversion rates in a more reliable calculation with higher angular resolution. This is intriguing since the calculations with higher resolution are barely accessible in multi-D SN models.

For the 27 $M_\odot$ progenitor model, no ELN crossings within the neutrino decoupling region were found. Although there exists a quadrupole structure in α, it is still too weak to result in the existence of regions with large α's. This comes as no surprise since the evolution of the multipole structures in neutrino emission depends sensitively on a number factors such as the mass of the progenitor, the treatment of neutrino transport, and even the employed EOS (see, e.g., Fig. 5 in Ref. [53]).

We point out that no ELN crossings were found in a recent self-consistent 2D SN simulation using the Furusawas EOS [84], as opposed to the Lattimer and Swesty EOS used in our calculations. This result is not inconsistent with the present study or with Ref. [56],

since convective motion, crucial to the existence and evolution of neutrino distribution asymmetries, is much weaker in the simulations with Furusawas EOS [59]. Therefore, one may expect to observe weaker distribution asymmetries in the simulation with the latter EOS.

Apart from the ELN crossings appearing within/above the neutrino decoupling region, our results show that there exist a class of ELN crossings that can occur in deep regions, well inside the PNS. We observed this sort of ELN crossing in both of the progenitor models we investigated. Because the neutrino angular distributions are extremely isotropic below the neutrinosphere, these ELN crossings can exist only within the zones where $\alpha \simeq 1$.

Needless to say, if ELN crossings and their corresponding fast modes actually occur in the SN environment and lead to significant flavor conversion, they can have profound consequences for the SN physics.

ACKNOWLEDGMENTS

S. A. and M. C. V. acknowledge support from Physique fondamentale et ondes gravitationelles (PhysFOG) of the Observatoire de Paris. H. D. is supported by U.S. DOE NP Grant No. DE-SC0017803 at UNM. This work is supported by Grant-in-Aid for Scientific Research (Grants No. 26104006, No. 15K05093, and No. 19K03837) and Grant-in-Aid for Scientific Research on Innovative areas "Gravitational wave physics and astronomy: Genesis" (Grants No. 17H06357 and No. 17H06365) from the Ministry of Education, Culture, Sports, Science and Technology (MEXT), Japan. For providing high performance computing resources, we acknowledge Computing Research Center, KEK, JLDG on SINET4 of NII, Research Center for Nuclear Physics, Osaka University, Yukawa Institute of Theoretical Physics, Kyoto University, Nagoya University, Hokkaido University, and Information Technology Center, University of Tokyo. This work was partly supported by research programs at K-computer of the RIKEN AICS, HPCI Strategic Program of Japanese MEXT, "Priority issue on post-K computer" (Elucidation of the Fundamental Laws and Evolution of the Universe) and Joint Institute for Computational Fundamental Sciences (JICFus).

[1] S. A. Colgate and R. H. White, The hydrodynamic behavior of supernovae explosions, Astrophys. J. **143**, 626 (1966).
[2] Y. Z. Qian and S. E. Woosley, Nucleosynthesis in neutrino driven winds: 1. The physical conditions, Astrophys. J. **471**, 331 (1996).
[3] H. A. Bethe and J. R. Wilson, Revival of a stalled supernova shock by neutrino heating, Astrophys. J. **295**, 14 (1985).
[4] H.-T. Janka, Explosion mechanisms of core-collapse supernovae, Annu. Rev. Nucl. Part. Sci. **62**, 407 (2012).
[5] A. Burrows, Colloquium: Perspectives on core-collapse supernova theory, Rev. Mod. Phys. **85**, 245 (2013).
[6] J. Gava, J. Kneller, C. Volpe, and G. C. McLaughlin, A Dynamical Collective Calculation of Supernova Neutrino Signals, Phys. Rev. Lett. **103**, 071101 (2009).
[7] S. Horiuchi, J. F. Beacom, and E. Dwek, The diffuse supernova neutrino background is detectable in Super-Kamiokande, Phys. Rev. D **79**, 083013 (2009).
[8] J. F. Beacom, The diffuse supernova neutrino background, Annu. Rev. Nucl. Part. Sci. **60**, 439 (2010).
[9] A. Mirizzi, I. Tamborra, H.-T. Janka, N. Saviano, K. Scholberg, R. Bollig, L. Hudepohl, and S. Chakraborty, Supernova neutrinos: Production, oscillations and setection, Riv. Nuovo Cimento **39**, 1 (2016).
[10] S. Horiuchi, K. Sumiyoshi, K. Nakamura, T. Fischer, A. Summa, T. Takiwaki, H.-T. Janka, and K. Kotake, Diffuse supernova neutrino background from extensive core-collapse simulations of 8–100 $M_\odot$ progenitors, Mon. Not. R. Astron. Soc. **475**, 1363 (2018).
[11] Y. Suwa, K. Sumiyoshi, K. Nakazato, Y. Takahira, Y. Koshio, M. Mori, and R. A. Wendell, Observing supernova neutrino light curves with Super-Kamiokande: Expected event number over 10 s, Astrophys. J. **881**, 139 (2019).
[12] S. Pastor and G. Raffelt, Flavor Oscillations in the Supernova Hot Bubble Region: Nonlinear Effects of Neutrino Background, Phys. Rev. Lett. **89**, 191101 (2002).
[13] H. Duan, G. M. Fuller, J. Carlson, and Y.-Z. Qian, Simulation of coherent nonlinear neutrino flavor transformation in the supernova environment. 1. Correlated neutrino trajectories, Phys. Rev. D **74**, 105014 (2006).
[14] H. Duan, G. M. Fuller, J. Carlson, and Y.-Z. Qian, Coherent Development of Neutrino Flavor in the Supernova Environment, Phys. Rev. Lett. **97**, 241101 (2006).
[15] H. Duan, G. M. Fuller, and Y.-Z. Qian, Collective neutrino oscillations, Annu. Rev. Nucl. Part. Sci. **60**, 569 (2010).
[16] S. Chakraborty, R. Hansen, I. Izaguirre, and G. Raffelt, Collective neutrino flavor conversion: Recent developments, Nucl. Phys. **B908**, 366 (2016).
[17] H. Duan, G. M. Fuller, J. Carlson, and Y.-Z. Qian, Flavor Evolution of the Neutronization Neutrino Burst from an O-Ne-Mg Core-Collapse Supernova, Phys. Rev. Lett. **100**, 021101 (2008).
[18] B. Dasgupta, A. Dighe, G. G. Raffelt, and A. Y. Smirnov, Multiple Spectral Splits of Supernova Neutrinos, Phys. Rev. Lett. **103**, 051105 (2009).
[19] S. Galais and C. Volpe, The neutrino spectral split in core-collapse supernovae: A magnetic resonance phenomenon, Phys. Rev. D **84**, 085005 (2011).
[20] H. Duan, G. M. Fuller, J. Carlson, and Y.-Z. Qian, Neutrino Mass Hierarchy and Stepwise Spectral Swapping of Supernova Neutrino Flavors, Phys. Rev. Lett. **99**, 241802 (2007).

[21] R. F. Sawyer, Speed-up of neutrino transformations in a supernova environment, Phys. Rev. D **72**, 045003 (2005).
[22] R. F. Sawyer, Neutrino Cloud Instabilities Just above the Neutrino Sphere of a Supernova, Phys. Rev. Lett. **116**, 081101 (2016).
[23] S. Chakraborty, R. S. Hansen, I. Izaguirre, and G. Raffelt, Self-induced neutrino flavor conversion without flavor mixing, J. Cosmol. Astropart. Phys. 03 (2016) 042.
[24] I. Izaguirre, G. Raffelt, and I. Tamborra, Fast Pairwise Conversion of Supernova Neutrinos: A Dispersion-Relation Approach, Phys. Rev. Lett. **118**, 021101 (2017).
[25] M.-R. Wu and I. Tamborra, Fast neutrino conversions: Ubiquitous in compact binary merger remnants, Phys. Rev. D **95**, 103007 (2017).
[26] F. Capozzi, B. Dasgupta, E. Lisi, A. Marrone, and A. Mirizzi, Fast flavor conversions of supernova neutrinos: Classifying instabilities via dispersion relations, Phys. Rev. D **96**, 043016 (2017).
[27] S. A. Richers, G. C. McLaughlin, J. P. Kneller, and A. Vlasenko, Neutrino quantum kinetics in compact objects, Phys. Rev. D **99**, 123014 (2019).
[28] B. Dasgupta, A. Mirizzi, and M. Sen, Fast neutrino flavor conversions near the supernova core with realistic flavor-dependent angular distributions, J. Cosmol. Astropart. Phys. 02 (2017) 019.
[29] S. Abbar and H. Duan, Fast neutrino flavor conversion: Roles of dense matter and spectrum crossing, Phys. Rev. D **98**, 043014 (2018).
[30] S. Abbar and M. C. Volpe, On fast neutrino flavor conversion modes in the nonlinear regime, Phys. Lett. B **790**, 545 (2019).
[31] F. Capozzi, B. Dasgupta, A. Mirizzi, M. Sen, and G. Sigl, Collisional Triggering of Fast Flavor Conversions of Supernova Neutrinos, Phys. Rev. Lett. **122**, 091101 (2019).
[32] J. D. Martin, C. Yi, and H. Duan, Dynamic fast flavor oscillation waves in dense neutrino gases arXiv:1909.05225.
[33] F. Capozzi, G. Raffelt, and T. Stirner, Fast neutrino flavor conversion: Collective motion vs. decoherence, J. Cosmol. Astropart. Phys. 09 (2019) 002.
[34] C. Döring, R. S. L. Hansen, and M. Lindner, Stability of three neutrino flavor conversion in supernovae, J. Cosmol. Astropart. Phys. 08 (2019) 003.
[35] M. Chakraborty and S. Chakraborty, Three flavor neutrino conversions in supernovae: Slow & fast instabilities, J. Cosmol. Astropart. Phys. 01 (2020) 005.
[36] L. Johns, H. Nagakura, G. M. Fuller, and A. Burrows, Neutrino oscillations in supernovae: Angular moments and fast instabilities, arXiv:1910.05682.
[37] V. Cirigliano, M. W. Paris, and S. Shalgar, Effect of collisions on neutrino flavor inhomogeneity in a dense neutrino gas, Phys. Lett. B **774**, 258 (2017).
[38] H. Duan and S. Shalgar, Flavor instabilities in the neutrino line model, Phys. Lett. B **747**, 139 (2015).
[39] S. Chakraborty, R. S. Hansen, I. Izaguirre, and G. Raffelt, Self-induced flavor conversion of supernova neutrinos on small scales, J. Cosmol. Astropart. Phys. 01 (2016) 028.
[40] S. Abbar, H. Duan, and S. Shalgar, Flavor instabilities in the multiangle neutrino line model, Phys. Rev. D **92**, 065019 (2015).
[41] S. Abbar and H. Duan, Neutrino flavor instabilities in a time-dependent supernova model, Phys. Lett. B **751**, 43 (2015).
[42] B. Dasgupta and A. Mirizzi, Temporal instability enables neutrino flavor conversions deep inside Supernovae, Phys. Rev. D **92**, 125030 (2015).
[43] R. S. L. Hansen and A. Y. Smirnov, Effect of extended neutrino production region on collective oscillations in supernovae, J. Cosmol. Astropart. Phys. 10 (2019) 27.
[44] I. Tamborra, L. Huedepohl, G. Raffelt, and H.-T. Janka, Flavor-dependent neutrino angular distribution in core-collapse supernovae, Astrophys. J. **839**, 132 (2017).
[45] S. Shalgar and I. Tamborra, On the occurrence of crossings between the angular distributions of electron neutrinos and antineutrinos in the supernova core, Astrophys. J. **883**, 80 (2019).
[46] T. Morinaga, H. Nagakura, C. Kato, and S. Yamada, A new possibility of the fast neutrino-flavor conversion in the preshock region of core-collapse supernova, arXiv:1909.13131.
[47] I. Tamborra, F. Hanke, H.-T. Janka, B. Müller, G. G. Raffelt, and A. Marek, Self-sustained asymmetry of lepton-number emission: A new phenomenon during the supernova shock-accretion phase in three dimensions, Astrophys. J. **792**, 96 (2014).
[48] D. Vartanyan, A. Burrows, and D. Radice, Temporal and angular variations of 3D core-collapse supernova emissions and their physical correlations, Mon. Not. R. Astron. Soc. **489**, 2227 (2019).
[49] K. Sugiura, K. Takahashi, and S. Yamada, Linear analysis of the shock instability in core-collapse supernovae: Influences of acoustic power and fluctuations of neutrino luminosity, Astrophys. J. **874**, 28 (2019).
[50] L. Walk, I. Tamborra, H.-T. Janka, and A. Summa, Effects of the standing accretion-shock instability and the lepton-emission self-sustained asymmetry in the neutrino emission of rotating supernovae, Phys. Rev. D **100**, 063018 (2019).
[51] R. Glas, H. T. Janka, T. Melson, G. Stockinger, and O. Just, Effects of LESA in three-dimensional supernova simulations with multi-Dimensional and ray-by-ray-plus neutrino transport, arXiv:1809.10150.
[52] E. P. O'Connor and S. M. Couch, Exploring fundamentally three-dimensional phenomena in high-fidelity simulations of core-collapse supernovae, Astrophys. J. **865**, 81 (2018).
[53] H. T. Janka, T. Melson, and A. Summa, Physics of core-collapse supernovae in three dimensions: A sneak preview, Annu. Rev. Nucl. Part. Sci. **66**, 341 (2016).
[54] I. Tamborra, G. Raffelt, F. Hanke, H.-T. Janka, and B. Mueller, Neutrino emission characteristics and detection opportunities based on three-dimensional supernova simulations, Phys. Rev. D **90**, 045032 (2014).
[55] H. Nagakura, K. Sumiyoshi, and S. Yamada, Possible early linear acceleration of protoneutron stars via asymmetric neutrino emission in core-collapse supernovae, Astrophys. J. **880**, L28 (2019).
[56] S. Abbar, H. Duan, K. Sumiyoshi, T. Takiwaki, and M. C. Volpe, On the occurrence of fast neutrino flavor conversions in multi-Dimensional supernova models, Phys. Rev. D **100**, 043004 (2019).

[57] K. Sumiyoshi and S. Yamada, Neutrino transfer in three dimensions for core-collapse supernovae. I. Static configurations, Astrophys. J. Suppl. Ser. **199**, 17 (2012).
[58] K. Sumiyoshi, T. Takiwaki, H. Matsufuru, and S. Yamada, multi-Dimensional features of neutrino transfer in core-collapse supernovae, Astrophys. J. Suppl. Ser. **216**, 5 (2015).
[59] H. Nagakura, W. Iwakami, S. Furusawa, H. Okawa, A. Harada, K. Sumiyoshi, S. Yamada, H. Matsufuru, and A. Imakura, Simulations of core-collapse supernovae in spatial axisymmetry with full Boltzmann neutrino transport, Astrophys. J. **854**, 136 (2018).
[60] M. D. Azari, S. Yamada, T. Morinaga, W. Iwakami, H. Okawa, H. Nagakura, and K. Sumiyoshi, Linear analysis of fast-pairwise collective neutrino oscillations in core-collapse supernovae based on the results of Boltzmann simulations, Phys. Rev. D **99**, 103011 (2019).
[61] H. Nagakura, T. Morinaga, C. Kato, and S. Yamada, Fast-pairwise collective neutrino oscillations associated with asymmetric neutrino emissions in core-collapse supernova, Astrophys. J. **886**, 139 (2019).
[62] M. D. Azari, S. Yamada, T. Morinaga, H. Nagakura, S. Furusawa, A. Harada, H. Okawa, W. Iwakami, and K. Sumiyoshi, Fast collective neutrino oscillations inside the neutrino sphere in core-collapse supernovae, Phys. Rev. D **101**, 023018 (2020).
[63] G. Sigl and G. Raffelt, General kinetic description of relativistic mixed neutrinos, Nucl. Phys. **B406**, 423 (1993).
[64] P. Strack and A. Burrows, A generalized boltzmann formalism for oscillating neutrinos, Phys. Rev. D **71**, 093004 (2005).
[65] C. Y. Cardall, Liouville equations for neutrino distribution matrices, Phys. Rev. D **78**, 085017 (2008).
[66] C. Volpe, D. Väänänen, and C. Espinoza, Extended evolution equations for neutrino propagation in astrophysical and cosmological environments, Phys. Rev. D **87**, 113010 (2013).
[67] A. Vlasenko, G. M. Fuller, and V. Cirigliano, Neutrino quantum kinetics, Phys. Rev. D **89**, 105004 (2014).
[68] L. Wolfenstein, Neutrino oscillations in matter, Phys. Rev. D **17**, 2369 (1978).
[69] S. P. Mikheyev and A. Y. Smirnov, Resonance amplification of oscillations in matter and spectroscopy of solar neutrinos, Sov. J. Nucl. Phys. **42**, 913 (1985).
[70] G. M. Fuller, R. W. Mayle, J. R. Wilson, and D. N. Schramm, Resonant neutrino oscillations and stellar collapse, Astrophys. J. **322**, 795 (1987).
[71] D. Nötzold and G. Raffelt, Neutrono dispersion at finite temperature and density, Nucl. Phys. **B307**, 924 (1988).
[72] J. T. Pantaleone, Dirac neutrinos in dense matter, Phys. Rev. D **46**, 510 (1992).
[73] A. Banerjee, A. Dighe, and G. Raffelt, Linearized flavor-stability analysis of dense neutrino streams, Phys. Rev. D **84**, 053013 (2011).
[74] D. Väänänen and C. Volpe, Linearizing neutrino evolution equations including neutrino-antineutrino pairing correlations, Phys. Rev. D **88**, 065003 (2013).
[75] P. A. Sturrock, Kinematics of growing waves, Phys. Rev. **112**, 1488 (1958).
[76] C. Yi, L. Ma, J. D. Martin, and H. Duan, Dispersion relation of the fast neutrino oscillation wave, Phys. Rev. D **99**, 063005 (2019).
[77] S. W. Bruenn, Stellar core collapse: Numerical model and infall epoch, Astrophys. J. Suppl. Ser. **58**, 771 (1985).
[78] J. M. Lattimer and F. D. Swesty, A generalized equation of state for hot, dense matter, Nucl. Phys. **A535**, 331 (1991).
[79] T. Takiwaki, K. Kotake, and Y. Suwa, Three-dimensional hydrodynamic core-collapse supernova simulations for an 11.2 $M_\odot$ star with spectral neutrino transport, Astrophys. J. **749**, 98 (2012).
[80] T. Takiwaki, K. Kotake, and Y. Suwa, A comparison of two- and three-dimensional neutrino-hydrodynamics simulations of core-collapse supernovae, Astrophys. J. **786**, 83 (2014).
[81] A. Harada, H. Nagakura, W. Iwakami, H. Okawa, S. Furusawa, H. Matsufuru, K. Sumiyoshi, and S. Yamada, On the neutrino sistributions in phase space for the rotating core-collapse supernova simulated with a Boltzmann-Neutrino-Radiation-Hydrodynamics code, Astrophys. J. **872**, 181 (2019).
[82] H. Duan, G. M. Fuller, and Y.-Z. Qian, A simple picture for neutrino flavor transformation in supernovae, Phys. Rev. D **76**, 085013 (2007).
[83] G. Mangano, A. Mirizzi, and N. Saviano, Damping the neutrino flavor pendulum by breaking homogeneity, Phys. Rev. D **89**, 073017 (2014).
[84] S. Furusawa, S. Yamada, K. Sumiyoshi, and H. Suzuki, A new baryonic equation of state at sub-nuclear densities for core-collapse simulations, Astrophys. J. **738**, 178 (2011).